Highlights:

1. Five data-driven control algorithms inspired by evolutionary game theory
2. Load balancing strategy for reallocation of available resources
3. Patented Neural Dynamic model optimizes the nonlinear design control parameters
4. Methodology increases the lifespan and reliability of semi-active devices
5. Advanced vibration mitigation of highway bridge structures subjected to earthquake loading

Load balancing and neural dynamic model to optimize replicator dynamic controllers for vibration reduction of highway bridge structures

Sajad Javadinasab Hormozabad[a], Mariantonieta Gutierrez Soto[a,*]

[a]*Department of Civil Engineering, University of Kentucky, 161 Raymond Building Lexington, KY 40506 U.S.A.*

Abstract

Earthquakes cause irreparable damages to the built environment, which has led bridge engineers to develop structural control systems to mitigate damage and improve vibration reduction in real-time. Among control systems, base isolation is one of the most commonly used passive control strategies for seismic protection of civil structures. Yet, it lacks real-time adaptability, has lower energy dissipation, and poor performance during near-fault earthquakes. To overcome these limitations, a hybrid control system comprised of semi-active magneto-rheological (MR) dampers and base isolation passive control is installed at the deck and piers for vibration reduction of highway bridge structures. This paper, inspired by evolutionary game theory and artificial intelligence, proposes data-driven replicator dynamic control algorithms to distribute the command voltage to the current driver of the semi-active MR dampers. It integrates a load balancing strategy to reallocate additional resources. To achieve a high-performance design of the game-theory inspired controllers, a patented Neural Dynamic model is used to optimize the control parameters. The evaluation of the proposed methodology uses a benchmark control problem based on the 91/5 highway bridge in Southern California subjected to near-field earthquake

*Corresponding author

Email addresses: sjavadinasab@uky.edu (Sajad Javadinasab Hormozabad), mariant.gutierrezsoto@uky.edu (Mariantonieta Gutierrez Soto)

URL: www.sotostructures.com (Mariantonieta Gutierrez Soto)

accelerograms. The performance of five different proposed controllers is compared with conventional Lyapunov and fuzzy logic control algorithms using 21 performance criteria. Results show the load balancing capability of the proposed control algorithms to mitigate the vibrations experienced by the bridge structure and further increase the durability of semi-active devices. The novelty of the methodology impacts how game-theory controllers make control decisions among multiple devices in engineering problems.

Keywords: Replicator dynamic, Game theory, Neural dynamic, Load balancing, Data-driven control, Structural control

1. INTRODUCTION

Civil infrastructure including bridges are vulnerable to man-made and natural hazard damages, which greatly affect the structural performance as well as the life-cycle costs [1, 2]. Extensive research about the economic consequences of failures and damages in bridges due to natural hazards, especially earthquakes, has highlighted the importance of vibration mitigation strategies for bridges [3, 4, 5]. Among different kinds of control systems used for seismic protection of bridges, base isolators are one of the most common systems [6]. Isolation systems increase the flexibility of the structures and therefore reduce the inertial force transferred from the ground to the structural elements [7, 8]. However, this kind of control system has its limitations. The isolated structures usually experience more significant relative deformations due to their increased flexibility [9]. For instance, the significant relative displacement between a bridge deck and pier can increase the damage and maintenance costs in an isolated bridge. On the other hand, the isolation systems show a relatively lower energy dissipation compared with viscous or MR dampers [10]. Furthermore, isolation bearings are not able to show adaptive performance in real time to improve the performance of control systems.

Accordingly, semi-active control devices like MR dampers can significantly increase the seismic performance of isolated bridges [11]. Different strategies have

been suggested to enhance the structural performance of seismically excited bridges. Fuzzy control algorithms are known as practical tools to deal with complex and nonlinear systems [12]. Eight different fuzzy rule bases for vibration control of bridge structures were proposed by Symans and Kelly [13]. A fuzzy supervisory control system was also implemented on a cable-stayed bridges by Park et al. [14]. Ok et al. [15] used a fuzzy control algorithm to determine the input voltage of MR dampers installed on cable-stayed bridges. Salari et al. [16] designed a variable Tuned Mass Damper (TMD) comprised of MR dampers for vibration mitigation of cable structures. The variable TMD incorporates fuzzy controllers to improve the performance of the proposed device.

Wang and Adeli [17] proposed a self-constructing wavelet neural network algorithm applicable for nonlinear control of large bridges. Zhang and Agrawal [18] investigated the energy dissipation patterns of MR dampers in semi-active and passive-on modes and proposed the "simple passive semi-active" control strategy for MR dampers. The authors numerically evaluated the effectiveness of the controller using the structural model of a three-story building. The results confirmed the satisfactory performance and robustness of the proposed control algorithm. AlHamaydeh et al. [19] proposed a Quasi-Bang-Bang algorithm for vibration reduction of a three-story linear frame structures using MR dampers. The frame structural model was subjected to ground motion accelerograms and the Quasi-Bang-Bang algorithm was optimized using a genetic algorithm. The authors concluded that the proposed optimized algorithm shows acceptable performance and is simple to implement. Javadinasab Hormozabad and Ghorbani-Tanha [20] evaluated the performance of data-driven fuzzy controllers using a 3D nonlinear model of Lali Cable-Stayed Bridge. According to the numerical results, the proposed semi-active controllers effectively reduced the seismic response of the bridge and showed promising robustness against time lag. Soares et al. [21] proposed a model-based adaptive control system for seismic protection of cable-stayed bridges. The system included MR dampers for energy dissipation together with a linear–quadratic regulator to determine the command voltage. The results showed the enhanced robustness of the pro-

posed system compared with passive and semi-active resettable devices made with pneumatic springs.

1.1. Model-based and data-driven control

Model-based adaptive controllers have been proposed for vibration control of structures [22]. Model-based controllers require an accurate analytical model of the structure which is commonly obtained through system identification and dynamic parameter estimation techniques. However, the estimation error leads to uncertainty in dynamic properties of the structural system which is known as system or model uncertainty [23]. The system uncertainty together with measurement uncertainty can lead to serious problems in terms of performance and robustness [24]. In addition, the dynamic properties of the structure may change with time which requires especial considerations for continuous model updating [25]. Therefore, there is a need for data-driven adaptive controllers, including those originated from artificial intelligence and game theory, which are model-free and make control decisions based on the measured data. Data-driven controllers are especially beneficial in cases where the analytical model of the controlled system is either unavailable, difficult to obtain, too complex for controller design, or containing serious uncertainties [24].

1.2. Game theory and load balancing

Zhang and Guizani [26] present noncooperative and cooperative games to efficiently solve resource allocation, power control, attack, routing, and energy management problems. The authors found that game theory is particularly useful in understanding complex interactions in wireless domains such as wireless sensor networks and vehicular networks, especially when there are limited resources such as bandwidth, power, and capacity. Bauso's [27] comprehensive book in game theory with engineering application introduces two-players zero-sum games, coalition games, evolutionary game theory, differential games, stochastic games, replicator dynamics, and learning in games. The author covers

the following engineering applications: multi-agent systems, demand-side management, synchronization of power generations, opinion dynamics, bargaining, supply chain, and cyber-physical systems with a human in the loop. Marden and Shamma [28] studied game theory applications in distributed control of engineering systems. Game theory was employed to improve intelligent transportation and traffic control systems [29, 30]. Despite its versatility, there is limited research studying game theory to solve structural engineering problems. This paper proposes novel data-driven controllers that integrate the evolutionary game theory, load balancing, and neural dynamic model to reduce vibrations of smart isolated bridge structures in real-time. Gutierrez Soto [31] proposed a hybrid control system for vibration mitigation of isolated bridges based on evolutionary game theory and replicator dynamics. This controller was employed to design a semi-active configuration for vibration control of isolated highway bridges [11]. Gutierrez Soto and Adeli [32] investigated vibration control of high-rise and base-isolated structures using game-theory inspired algorithms that were optimized using the patented Neural Dynamic (ND) model of Adeli and Park [33, 34, 35]. The results showed that the optimal Replicator Dynamics Controller (RDC) makes a remarkable reduction in seismic response of the bridge, especially the midspan displacement of the deck. Sohrabi and Azgomi [36] combined game theory and optimization methods for its application in control systems. In a multi-agent system designed to perform a specific task, load balancing or reallocation strategies are used to redistribute the task over underloaded agents so that no agent will be overloaded and the task will be carried out with higher efficiency [37]. [38] reviewed deterministic and non-deterministic load balancing mechanisms in software-defined networks.

In this paper, a new load balancing strategy is proposed for the semi-active control methodology. This strategy allows for the modification of resource allocation process by adding a voltage redistribution strategy to prevent any MR damper from being overloaded and assign the remaining voltage to the other devices. The load balancing strategy improves the performance of the game-theory inspired RDCs and reduces the required voltage supply.

- Fitness functions are devised to develop five evolutionary game theory-based data-driven controllers.
- A load balancing strategy is proposed for effective reallocation in real-time of available resources.
- Introduces five semi-active data-driven control systems incorporating the RDCs together with the load balancing strategy for semi-active vibration reduction of highway bridge structures.
- Optimizes control parameters studying the U.S. patented neural dynamic model to optimize the design of the proposed RDCs

The proposed RDCs are implemented on the benchmark problem for an isolated highway bridge subjected to seismic loading. Then, the performance of the proposed control methodology is evaluated and compared to conventional Lyapunov-based and fuzzy control algorithms.

2. METHODOLOGY

2.1. Equations of motion

The dynamic equation of motion for the isolated bridge equipped with semi-active MR dampers is presented below.

$$\mathbf{M}\ddot{\mathbf{u}}(t) + \mathbf{C}\dot{\mathbf{u}}(t) + \mathbf{K}\mathbf{u}(t) = -\mathbf{M}\boldsymbol{\theta}\ddot{u}_g(t) + \mathbf{R}\mathbf{r}(t) + \mathbf{W}\mathbf{w}(t) \tag{1}$$

where $\mathbf{u}$ is the bridge displacement vector. $\mathbf{M}$, $\mathbf{C}$, and $\mathbf{K}$ are respectively the bridge mass, damping, and stiffness matrices; $\boldsymbol{\theta}$ is a vector which determines how the inertial force acts on the bridge; $\ddot{u}_g(t)$ contains the ground acceleration in two perpendicular directions. $\mathbf{R}$ and $\mathbf{W}$ are the influence matrices respectively affecting the semi-active control force, $\mathbf{r}$(t), and the passive (isolation) control

force, $\mathbf{w}$(t). This equation can be converted to the state space form as presented in Equation 2.

$$\dot{\mathbf{x}}(t) = \begin{bmatrix} \dot{\mathbf{u}}(t) \\ \mathbf{u}(t) \end{bmatrix} = \mathbf{A}\mathbf{x}(t) + \mathbf{B}_r\mathbf{z}_r(t) + \mathbf{B}_w\mathbf{z}_w(t) + \mathbf{E}\ddot{u}_g(t) \tag{2}$$

where $\mathbf{x}(t)$ is the state variable vector, $\mathbf{B}_r$ and $\mathbf{B}_w$ are the control force matrices corresponding to $\mathbf{z}_r(t)$ and $\mathbf{z}_w(t)$, respectively. $\mathbf{A}$, $\mathbf{B}_r$, $\mathbf{B}_w$, $\mathbf{E}$, $\mathbf{z}_r$, and $\mathbf{z}_w$ are formulated as:

$$\mathbf{A} = \begin{bmatrix} [\mathbf{0}] & [\mathbf{I}] \\ -\mathbf{M}^{-1}\mathbf{K} & -\mathbf{M}^{-1}\mathbf{C} \end{bmatrix} \tag{3}$$

$$\mathbf{B}_r = \begin{bmatrix} [\mathbf{0}] \\ -\mathbf{M}^{-1}\mathbf{R} \end{bmatrix} \tag{4}$$

$$\mathbf{B}_w = \begin{bmatrix} [\mathbf{0}] \\ -\mathbf{M}^{-1}\mathbf{W} \end{bmatrix} \tag{5}$$

$$\mathbf{E} = \begin{bmatrix} [\mathbf{0}] \\ \boldsymbol{\theta} \end{bmatrix} \tag{6}$$

$$\mathbf{z}_r = \begin{bmatrix} [\mathbf{0}] \\ \mathbf{r}(t) \end{bmatrix} \tag{7}$$

$$\mathbf{z}_w = \begin{bmatrix} [\mathbf{0}] \\ \mathbf{w}(t) \end{bmatrix} \tag{8}$$

The output vector, $\mathbf{y}(t)$, is obtained through Equation 9.

$$\mathbf{y}(t) = \mathbf{T}\mathbf{x}(t) + \mathbf{D}\begin{bmatrix} \mathbf{z}_r \\ \mathbf{z}_w \end{bmatrix} + \mathbf{L}_g\ddot{u}_g(t) \tag{9}$$

where $\mathbf{T}$ is the output matrix, $\mathbf{D}$ is the feedforward matrix affecting the control force vector, and $\mathbf{L}_g$ is the feedforward vector that contains the ground acceleration.

2.2. Replicator Dynamics Methodology

According to the biological concept of evolutionary game theory, the selection in a population is affected by the fitness of each individual. Fitness shows an individual's rate of success to reproduce and develop his generation. In other words, individuals with higher fitness deserve more population in the next generation [39]. This theory can be adopted in order to establish resource allocation problem-solving models for engineering applications. In a typical resource allocation problem, a limited resource (in this case the voltage resource) must be allocated to several consumers in such a way as to follow a specific goal. Each consumer is assigned a fitness function describing its capability to receive the voltage. Then the fitness values of different consumers are compared to each other and those with higher fitness receive larger voltage.

Replicator dynamics is a methodology for dealing with resource allocation problems. It uses a specific rule to generate different generations of data. In this research, replicator dynamics based on evolutionary game theory is used to control the structural response of an isolated highway bridge. For this purpose, the control devices installed on the bridge (herein the MR dampers) take the position of the consumers and the total available amount of electrical voltage is allocated to the dampers. Therefore, the population vector at time t denoted by $\mathbf{v}(t)$ can be presented as:

$$\mathbf{v}(t) = \begin{bmatrix} V_1(t) \\ \vdots \\ V_N(t) \end{bmatrix} \tag{10}$$

where $V_i(t)$ denotes the command voltage to the current driver of the i^{th} MR damper and N is the total number of MR dampers. In order to obtain the variation of the population vector, a weighted average of fitness functions is defined as follows:

$$\phi(t) = \frac{1}{V_T} \sum_{i=1}^{N+1} V_i(t) f_i(t) \tag{11}$$

where $f_i(t)$ is the fitness function for the i^{th} MR damper and V_T is the total

available voltage. Based on replicator dynamics [40], f_{N+1} is defined as the fitness function of the fictitious device, and set to a very small positive number to absorb the voltage recourse when the structure is not in motion. Following the game theory concept, the fictitious device is the device closer to *winning* the game and the one that all other devices aim to replicate. Now, the variation of the command voltage to the current driver for each MR damper is obtained through the following replication equation:

$$\dot{V}_i(t) = \beta V_i(t)[f_i(t) - \phi(t)] \qquad \text{for} \quad i = 1, \ldots, N+1 \tag{12}$$

where β is the growth rate and determines how fast the population vector components change over time t. Equation 12 shows that the variation of the input voltage for MR dampers with a fitness function larger than the average is positive. Contrarily, the dampers with fitness functions smaller than the average value are receiving decaying input voltages.

The bridge responses sensed at different locations on the bridge play the key role in defining the fitness functions. In other words, the part of the bridge experiencing a more significant response needs a relatively larger damping force to mitigate the dynamic response. Accordingly, the sensor measurements at control devices should be considered to define the fitness functions. In the present study, five different fitness functions are devised to develop five RDCs. The fitness functions are defined as follows:

$$f_i^{(j)}(t) = \begin{cases} Q_i^{(j)}(t), & \text{if} \quad i = 1, ..., N,\ j = 1, ..., N_c \qquad (13) \\ 1.0\text{x}10^{-3}, & \text{if} \quad i = N+1,\ j = 1, ..., N_c \qquad (14) \end{cases}$$

where $Q_i^{(j)}(t)$ is the measurement at the i^{th} location using the j^{th} RDC. In this study, five (5) proposed controllers are investigated ($N_c = 5$). Table 1 describes the measurements used to obtain fitness function of the j^{th} RDC. In this table, u denotes the displacement response of the bridge as a function of time. $Q_i^{(j)}$ is also described as a function of time and measured structural response. The overall configuration of the RDCs proposed for isolated bridge structures is illustrated in Figure 1.

Table 1: Definition of sensor measurements used to define fitness functions in different RDCs

RDC	Measurement	Description
RDC 1	$Q_i^{(1)}(t) = \lvert\ddot{u}_{deck}(t) - \ddot{u}_{abt}(t)\rvert$	Relative acceleration across the damper
RDC 2	$Q_i^{(2)}(t) = \lvert\ddot{u}_{deck}(t)\rvert$	Absolute acceleration of the deck
RDC 3	$Q_i^{(3)}(t) = \lvert\dot{u}_{deck}(t) - \dot{u}_{abt}(t)\rvert$	Relative velocity across the damper
RDC 4	$Q_i^{(4)}(t) =$ $[\dot{u}_{deck}(t) - \dot{u}_{abt}(t)] \cdot [u_{deck}(t) - u_{abt}(t)]$	Relative velocity multiplied by the relative displacement
RDC 5	$Q_i^{(5)}(t) = \begin{cases} -1, & \text{if} \quad [\cdot] < 0 \\ 0, & \text{if} \quad [\cdot] = 0 \\ 1, & \text{if} \quad [\cdot] > 0 \end{cases}$ where $[\cdot] = \lvert\dot{u}_{deck}(t) - \dot{u}_{abt}(t)\rvert \cdot \lvert u_{deck}(t) - u_{abt}(t)\rvert$	The sign of multiplication of relative velocity and displacement

2.3. Load Balancing

As described earlier, RDCs allocate the total voltage to control devices based on their instantaneous fitness function. Accordingly, control devices with higher fitness function receive larger input voltage and, in some cases, the voltage allocated to a device can be larger than its capacity. Particularly, considering V_{max} as the maximum input voltage capacity of an MR damper, there is a time t where the sensor measurements at the i^{th} location lead the algorithm to allocate voltage larger than V_{max}. When the device receives a command voltage larger than V_{max}, V_{max} is applied and the excessive voltage is not redistributed properly over the rest of control devices.

To resolve this issue, a load balancing strategy is devised in the present

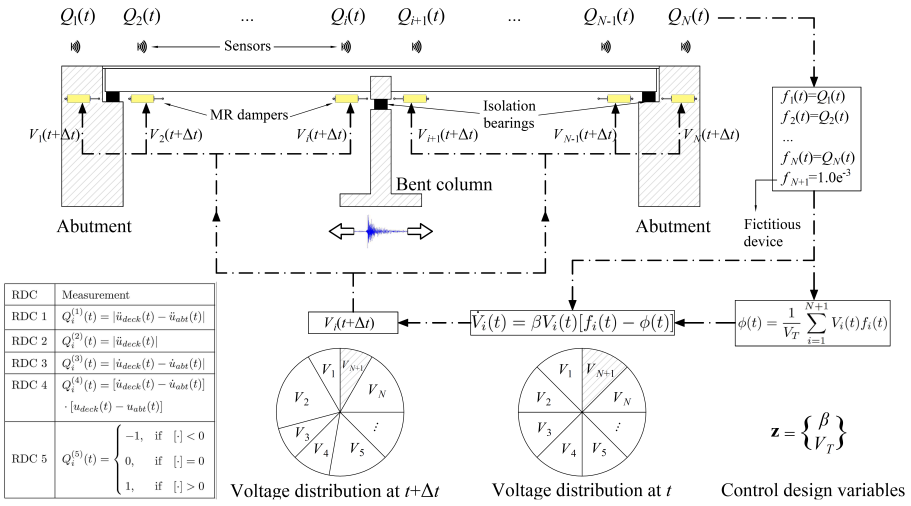

Figure 1: Overall configuration of the RDCs proposed for the bridge structure

study to modify the distribution of the voltage resource. Accordingly, each time a device is overloaded, the corresponding fitness function is modified so that its value is decreased. Consequently, the voltage distribution is balanced, and the additional available voltage is redistributed over under-loaded devices. To implement the load balancing strategy in proposed RDCs, the fitness functions are modified based on the following equation. The second term in this equation reduces the fitness function for those control devices that are over-allocated.

$$f_i^{(j)_m}(t) = Q_i^{(j)}(t) + G_b \frac{\min\left[V_i(t), V_{max}\right] - V_i(t)}{V_e(t)}, \qquad i = 1, ..., N \tag{15}$$

where $f_i^{(j)_m}(t)$ denotes the modified fitness function and G_b is a constant that modulates the load balancing strategy. $V_e(t)$ is the additional available voltage and is obtained through the following equation:

$$V_e(t) = \sum_{i=1}^{N} \{V_i(t) - \min[V_i(t), V_{max}]\} \tag{16}$$

Once the modified fitness functions are obtained, the modified values of average fitness function and the selection dynamics, respectively denoted by $\phi^m(t)$ and $\dot{V}_i^m(t)$, are calculated through Equations 17 and 18.

$$\phi^m(t) = \frac{1}{V_T} \sum_{i=1}^{N+1} V_i(t) f_i^{(j)_m} \tag{17}$$

$$\dot{V}_i^m(t) = \beta V_i(t)[f_i^{(j)_m}(t) - \phi^m(t)], \qquad i = 1, ..., N \tag{18}$$

Figure 2 illustrates the architecture of the control system including the RDC and the load balancing strategy. According to Figures 1 and 2, the proposed control strategy encompasses the following steps which are repeated in real-time during each sampling interval.

1. The seismic response data are measured through the sensory system and fed into the RDC.
2. The fitness function for each MR damper is calculated through Equations 13 and 14 according to the selected fitness function, $Q_i(t)$, in Table 1 defining each replicator dynamic controller.
3. The weighted average of allocated voltage and fitness functions (ϕ) is calculated through Equation 11.
4. The command voltage for each MR damper is calculated through Equation 12 and fed into the load balancing block.
5. The additional available voltage (V_e) is calculated through Equation 16.
6. The modified fitness function for each MR damper is calculated through Equation 15.
7. The modified weighted average of fitness functions (ϕ^m) is calculated through Equation 17.
8. The modified command voltage for each MR damper is calculated through the replicator dynamics equation (Equation 18) and fed into the current driver of corresponding MR damping device.

2.4. Fuzzy Controller

Fuzzy inference systems provide flexible tools to deal with control problems because the algorithm is compatible with the human reasoning language and

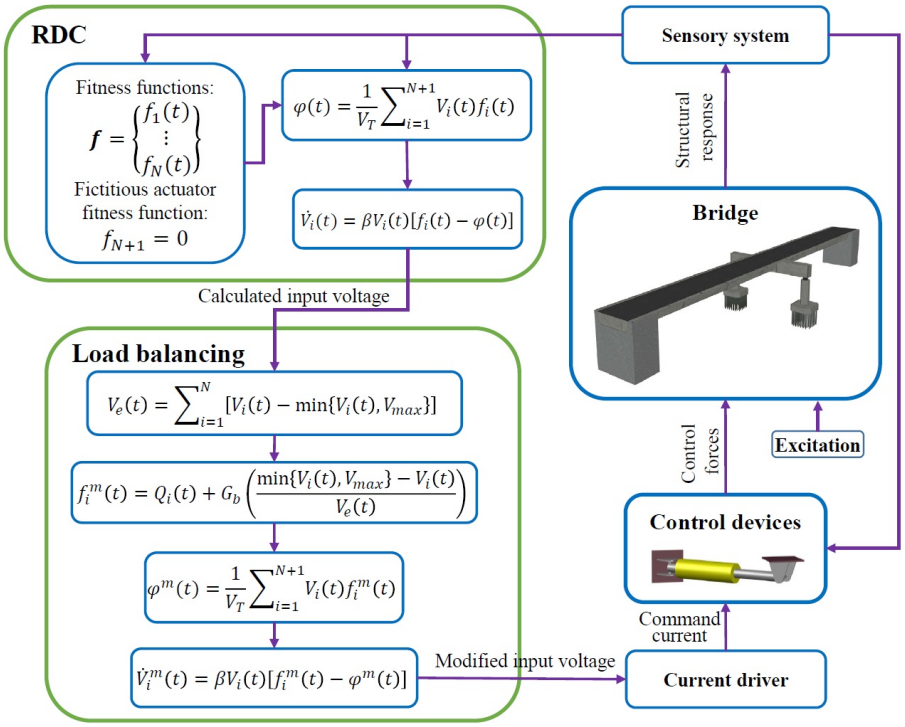

Figure 2: Overall configuration of control system including the RDC and the load balancing (resource reallocating) strategy

effectively manages the if-then rules. Fuzzy controllers have a data-driven configuration and show promising performance to handle complicated and nonlinear systems [41]. Fuzzy controllers are effective in a decentralized architecture because the outputs can be directly obtained from local structural response data defined as the inputs to the fuzzy algorithm. Game theory-based controllers are also data-driven and use mathematical modeling of cooperation and competition among rational individuals. Based on these characteristics, this study will compare these innovative approaches with a soft computing method based on fuzzy logic that is a conventional approach accepted in current practice, data-driven, and designed with human reasoning language. Accordingly, a fuzzy controller based on a type-1 Mamdani fuzzy inference system is proposed as a semi-active alternative to perform the comparative study. In order to implement the fuzzy

control algorithm, the fuzzy rule-base proposed by Ok et al. [15] is modified to be used for the benchmark isolated highway bridge. In the proposed fuzzy strategy, the measured response data are first fed into the fuzzification process. Considering the relative velocity across the MR dampers as the input variable, 11 fuzzy sets including NVL, NL, NM, NS, NVS, ZO, PVS, PS, PM, PL, and PVL are defined. The letters N, ZO, and P stand for negative, zero, and positive, respectively. V stands for very and L, M, and S respectively stand for large, medium and small. Then the fuzzy inputs are processed through a fuzzy rule table which regulates the relationship between the fuzzy input and outputs. Afterwards, the fuzzy outputs are obtained and fed into the defuzzification process to be converted to actual outputs based on the output fuzzy sets. In the present study, a centroid method is utilized for defuzzification. The command voltage of the MR damper is regarded as the output of the fuzzy inference system and six fuzzy sets including VL, L, M, S, VS, and ZO are defined for defuzzification procedure. The fuzzy sets and corresponding membership functions defined for input and output variables are graphically presented in Figure 3. The rule table used for the inference system is also presented in Table 2.

Table 2: Tabular presentation of the rule-base used in the fuzzy controller

	Relative velocity across MR damper, $[\dot{u}_{deck}(t) - \dot{u}_{abt}(t)]$										
	NVL	NL	NM	NS	NVS	ZO	PVS	PS	PM	PL	PVL
Command voltage, $V_i(t)$	VL	L	NL	S	VS	ZO	VS	S	M	L	VL

2.5. Optimization via Neural Dynamic Model

The numerical model of the proposed system is comprised of the finite element model of the bridge structure, nonlinear model of passive and semi-active control devices, measurement simulations, and control strategy algorithm. Therefore, the optimization algorithm must be competent enough to handle such complicated numerical model and effectively optimize the parameters of the proposed RDCs. Accordingly, the patented Neural Dynamic model of Adeli and

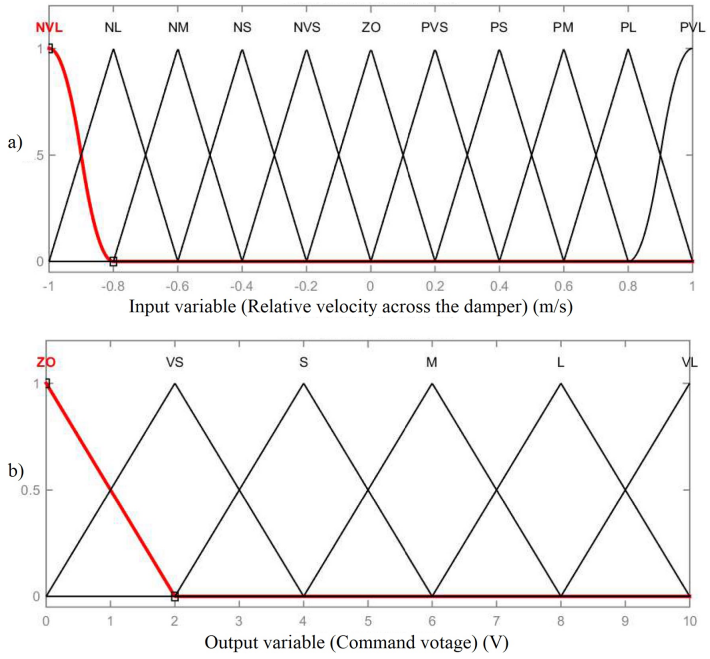

Figure 3: The membership function of different fuzzy sets related to a) input and b) output variables

Park (U.S. patent 5,815,394 issued date on September 29, 1998) is investigated in the present study to determine optimal game-theory based control parameters. Showing a robust performance for nonlinear and large-scale problems is one of the advantages of this method [42, 43]. Implementation of this method together with the Lyapunov stability theorem as well as the Karush-Kuhn-Tucker (KKT) conditions guarantees the global convergence of optimization process [34]. The topology of the neural dynamic model used to optimize the RDCs is presented in Figure 4.

A typical optimization problem can be mathematically represented as follows.

Minimize $F(\mathbf{z})$ subjected to

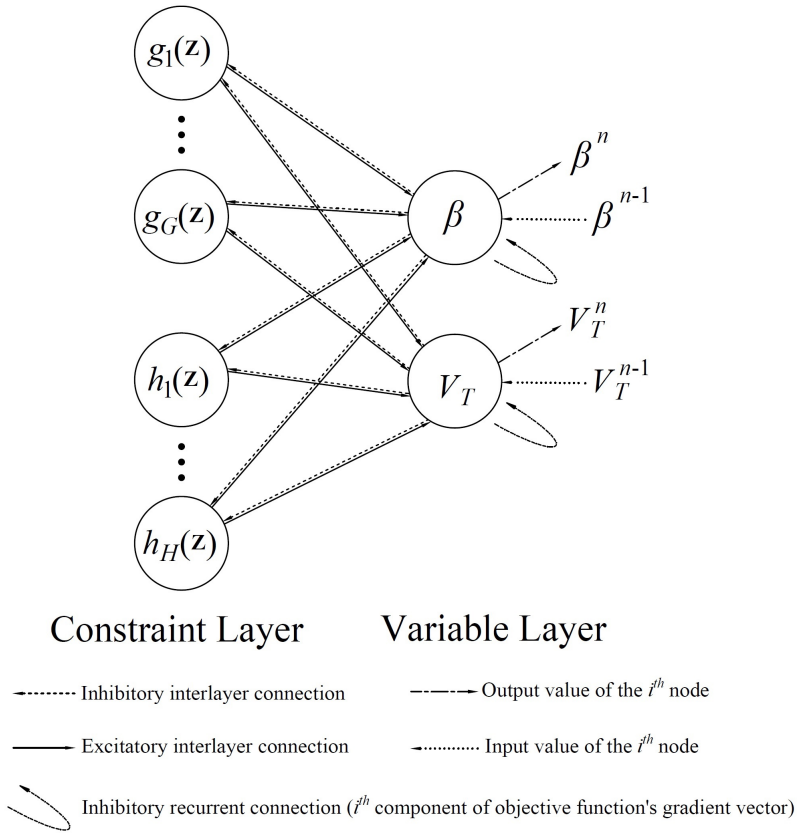

Figure 4: Topology of the neural dynamic model for optimizing the RDCs

$$g_j(\mathbf{z}) \leq 0 \qquad j = 1, ..., G \tag{19}$$

$$h_k(\mathbf{z}) = 0 \qquad k = 1, ..., H \tag{20}$$

where $\mathbf{z}$ is the state vector comprised of design variables, $g_j(\mathbf{z})$ and $h_k(\mathbf{z})$ represent the j^{th} inequality and the k^{th} equality constraints, respectively. G and H are the number of inequality and equality constraints, respectively. According to KKT conditions, the inequalities in Equation 19 are converted to their corresponding equalities as presented in Equation 21.

$$g_j(\mathbf{z}) + \omega_j^2 = 0 \qquad j = 1, ..., G \tag{21}$$

A Lagrange function including the constraints and the objective function is then defined using λ, α and γ as Lagrange multipliers (Equation 22).

$$L(\mathbf{z}, \lambda, \alpha, \gamma, \omega) = \sum_{m=1}^{M} \lambda_m \nabla F_m(\mathbf{z}) + \sum_{j=1}^{G} \alpha_j \left[g_j(\mathbf{z}) + \omega_j^2 \right] + \sum_{k=1}^{H} \gamma_k h_k(\mathbf{z}) \tag{22}$$

By adding a penalty function to Equation 22, the Lagrange function can be restated in Equation 23.

$$L(\mathbf{z}, r_n) = \sum_{m=1}^{M} \lambda_m \nabla F_m(\mathbf{z}) + \frac{r_n}{2} \left\{ \sum_{j=1}^{G} \left[g_j^+(\mathbf{z}) \right]^2 + \sum_{k=1}^{H} \left[h_k(\mathbf{z}) \right]^2 \right\} \tag{23}$$

Where $g_j^+(\mathbf{z}) = \max_j\{0, g_j(\mathbf{z})\}$ and r_n is the exterior penalty parameter defined as:

$$r_n = r_0 + \frac{n_i}{\epsilon} \tag{24}$$

Where, r_0 is the initial penalty parameter, and ϵ is a strictly positive number dependent on the optimization problem. n_i is the iteration number. Obtaining the derivative of both sides of Equation 23 gives:

$$\begin{array}{l} \frac{dL}{dt} = \dot{L}(\mathbf{z}, r_n) = \\ \left\{ \sum_{m=1}^{M} \lambda_m \frac{\partial F_m(\mathbf{z})}{\partial \mathbf{z}} + r_n \left[\sum_{j=1}^{G} g_j^+(\mathbf{z}) \frac{\partial g_j(\mathbf{z})}{\partial \mathbf{z}} + \sum_{k=1}^{H} [h_k(\mathbf{z}) \frac{\partial h_k(\mathbf{z})}{\partial \mathbf{z}} \right] \right\} \left(\frac{\partial \mathbf{z}}{\partial t} \right) = \\ \left\{ \sum_{m=1}^{M} \lambda_m \nabla F_m(\mathbf{z}) + r_n \left[\sum_{j=1}^{G} g_j^+(\mathbf{z}) \nabla g_j(\mathbf{z}) + \sum_{k=1}^{H} [h_k(\mathbf{z}) \nabla h_k(\mathbf{z}) \right] \right\} \dot{\mathbf{z}} \end{array} \tag{25}$$

where ∇ denotes the gradient, and the variation of state vector is obtained through Equation 26.

$$\dot{\mathbf{z}} = -\sum_{m=1}^{M} \lambda_m \nabla F_m(\mathbf{z}) - r_n \left[\sum_{j=1}^{G} g_j^+(\mathbf{z}) \nabla g_j(\mathbf{z}) - \sum_{k=1}^{H} h_k(\mathbf{z}) \nabla h_k(\mathbf{z}) \right] \tag{26}$$

By substituting $\dot{\mathbf{z}}$ (Equation 26) into Equation 25, $\dot{L}$ can be restated as:

$$\dot{L} = -\left| \sum_{m=1}^{M} \lambda_m \nabla F_m(\mathbf{z}) + r_n \left[\sum_{j=1}^{G} g_j^+(\mathbf{z}) \nabla g_j(\mathbf{z}) + \sum_{k=1}^{H} h_k(\mathbf{z}) \nabla h_k(\mathbf{z}) \right] \right|^2 \tag{27}$$

Equation 27 shows that the derivative of the Lagrange function is always negative, and the stability of the dynamic system is guaranteed. Accordingly, the equilibrium point can be calculated using a fourth order Runge-Kutta method through Equation 28.

$$\mathbf{z} = \int \dot{\mathbf{z}} dt \tag{28}$$

The following describes the optimization problem in terms of the design variables, constraints, and objective function.

2.5.1. Design variables

The design variables of the optimization problem include the total available voltage (V_T) and the growth rate (β).

2.5.2. Objective function

In order to maximize the performance of the controller, an objective function is defined in order to minimize the average value of the first three performance criteria (Equation 29). J_1 to J_3 respectively describe the peak base shear, peak overturning moment, and peak mid-span displacement in controlled bridge normalized by the corresponding values in uncontrolled bridge.

$$F(\mathbf{z}) = \frac{\sum_{i=1}^{3} J_i}{3} \tag{29}$$

2.5.3. Constraints

The total available voltage is considered to vary in $(0, V_T^{max})$ interval and the growth rate should have a positive value. Therefore, the constraints can be expressed mathematically through the following equations.

$$g_1(\mathbf{z}) : V_T - V_T^{max} \leq 0 \tag{30}$$

$$g_2(\mathbf{z}) : -V_T < 0 \tag{31}$$

$$g_3(\mathbf{z}) : -\beta \leq 0 \tag{32}$$

3. MODEL

In the present study, the proposed control methodology is evaluated using an isolated highway bridge structure subjected to earthquake loading. The structural model of the bridge as well as the model of the control system components are created in MATLAB and SIMULINK. The following describes the bridge and the control device model.

3.1. Bridge model

The benchmark control problem proposed by Nagarajaiah et al. [44] is used to evaluate the proposed load balancing RDC methodologies. This problem is defined based on the actual 91/5 highway bridge equipped with fluid viscous dampers and isolation systems constructed in Southern California subjected to near-field earthquake accelerograms. The bridge finite element model includes 108 nodes, 430 DOF, 70 beam elements, 4 rigid links, 24 springs, 8 bearings at abutments, and 27 dashpots [45].

To control the dynamic response of the bridge, 20 MR dampers are included at 10 different locations in the bridge model. The overall configuration of the benchmark bridge is illustrated in Figure 5. Figure 6 presents the 3D view of the MR dampers connecting the deck to the abutments. The layout of the bent column and the isolation bearings is shown in Figure 7. The arrangement of control devices and sensors is also demonstrated in Figure 8.

3.2. MR damper model

In order to simulate the behavior of MR dampers, the Bouc-Wen model proposed by Jansen and Dyke [46] is employed. Accordingly, the damping force F_d is obtained through the following equations:

$$F_d(t) = C_0\dot{u}(t) + az_d(t) \tag{33}$$

$$\dot{z}_d(t) = -\gamma_d z_d(t)\,|\dot{u}(t)|\,|z_d(t)|^{n-1} - \beta_d\dot{u}(t)\,|z_d(t)|^n + A_m\dot{u}(t) \tag{34}$$

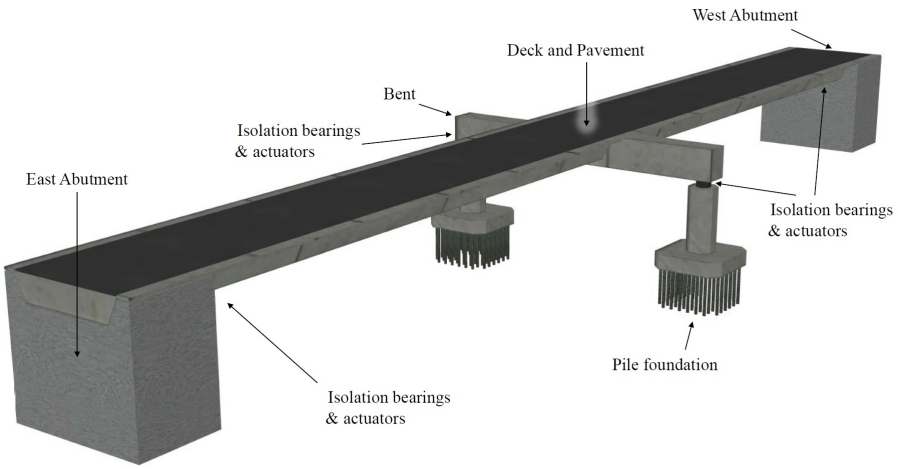

Figure 5: Overall configuration of the benchmark bridge

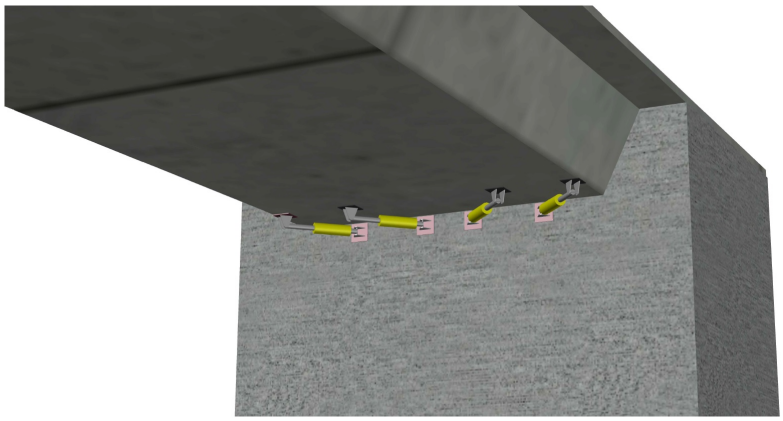

Figure 6: 3D view of the MR dampers installed between the deck and abutment

where, $u(t)$ is the displacement of the damper and $z_d(t)$ is the evolutionary variable. γ_d, β_d, n, and A_m are constant values obtained through experiments. C_0 and a are defined based on the control voltage ν through the following equations:

$$a = a(\nu) = a_a + a_b\nu \tag{35}$$

$$C_0 = C_0(\nu) = C_{0a} + C_{0b}\nu \tag{36}$$

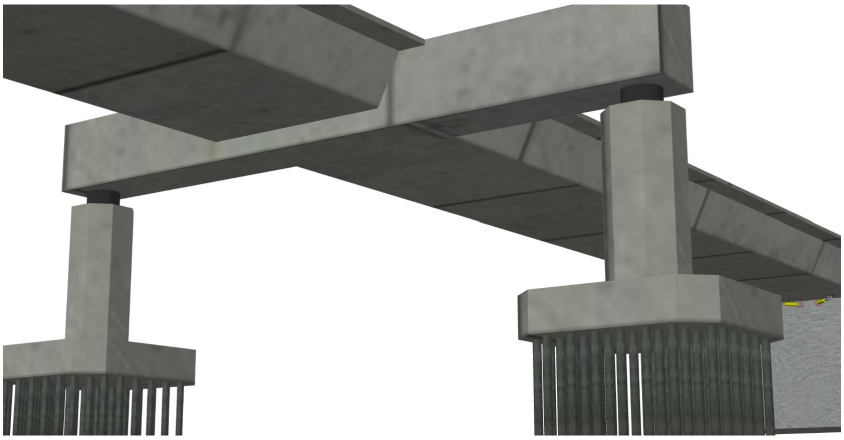

Figure 7: 3D view of the bent column and the isolation bearings

where ν is the applied control voltage to the current driver and other parameters including a_a, a_b, C_{0a}, and C_{0b} are specified through experiments. The time lag related to applying the command voltage is simulated using the following first-order filter with a time constant of η:

$$\dot{\nu} = -\eta\,(\nu - V) \tag{37}$$

Where, V is the command voltage applied to the current driver of the MR damper. To determine the parameters of MR dampers based on a feasible and practical configuration, the experimental study conducted by Yi et al. [47] is considered. Then, the parameters are scaled up to get a maximum damping force capacity of 1,000 kN with a maximum command voltage of 10 V, as suggested by Tan and Agrawal [48]. The parameters used for MR damper model are presented in Table 3.

4. EVALUATION OF PERFORMANCE

Nonlinear time history analyses are employed to obtain the dynamic response of the bridge subjected to four near-fault records. Table 4 presents the properties of these earthquake records. To synchronize the control system with

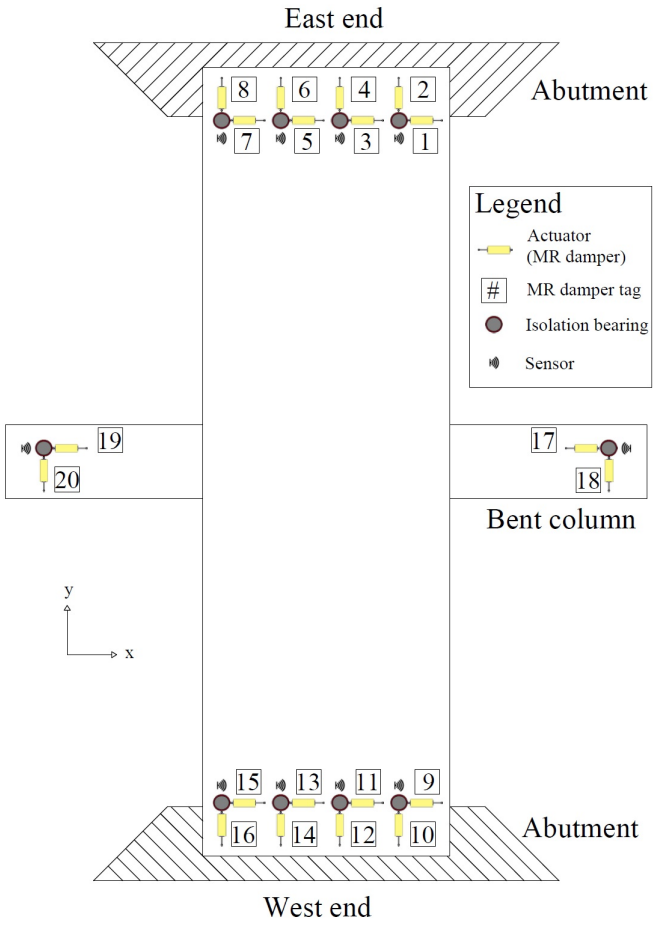

Figure 8: Arrangement of the benchmark control system components

the measured dynamic responses, the sampling time of the proposed digital controllers is set equal to the integration step of the simulation. The A/D and D/A converters on the digital controller have 16-bit precision and a span of ± 10 V. A root mean-square noise of 0.03 V (0.3% of the full span of the A/D converters) is included in the measured responses. Rectangular pulses with Gaussian distribution are considered for the measurement noises. The pulse width is also set equal to the integration step. The performance of each controller is then evaluated using 21 different performance criteria suggested by Agrawal et al.

Table 3: The parameters used to simulate the mechanical behavior of MR dampers (adapted from Yi et al. [47] and Tan and Agrawal [48])

Parameter	Value	Unit
a_a	1.0872×10^5	N/cm
a_b	4.9616×10^5	N/(cm.V)
C_{0a}	4.40	N.s/cm
C_{0b}	44.0	N.s/(cm.V)
γ_d	3.0	cm^{-1}
β_d	3.0	cm^{-1}
n	1.0	-
A_m	1.2	-
η	50.0	s^{-1}

[45]. These performance criteria are described in Table 10 in Appendix A.

Table 4: Characteristics of the near-fault earthquake records used to carry out the time history analyses (adapted from Agrawal et al. [45])

Station	EQ	Year	Peak acceleration (g)		Peak velocity (cm/s)	
			EW component	NS component	EW component	NS component
TCU084	Chi-Chi	1999	1.157	0.417	114.7	45.6
El Centro	Imperial Valley	1940	0.313	0.215	29.8	30.2
Bolu	Duzce, Turkey	1999	0.728	0.822	166.1	62.1
Nishi-Akashi	Kobe	1995	0.509	0.503	37.3	36.6

4.1. Computational complexity and implementation costs

To determine the optimal parameters of the RDCs, two interconnected numerical models are studied simultaneously: the neural dynamic model and the structural simulation model. At each iteration of the optimization algorithm, the structure's dynamic performance is evaluated. Considering the highly complex finite element model of the structure and the proposed nonlinear control systems, the optimization and structural models' calculation speed is essential. The convergence and rate of analysis in neural networks requires special considerations when studying a highly nonlinear problem. The patented neural dynamic model adds a penalty function method, Lyapunov stability theorem, Kuhn-Tucker conditions to handle nonlinearities in the optimization process. Making an appropriate balance between Lagrange multiplier λ_m and the penalty function r_n is the key to prevent divergence and save computational effort. Although the optimization procedure has its challenges and computational costs, the controller's numerical model is efficient enough to work in real-time once the controller is optimized. Moreover, the proposed data-driven controllers do not rely on the structural model. The control decisions are computed based on the dynamic response data, which can be processed very quickly through the proposed RDC formulation. In general, the numerical simulations show that the computation time for each step of analysis is negligible. The controller works efficiently in real-time with other components of the control system, including the MR dampers. Investigations have shown that the semi-active control systems with MR dampers are bounded-input and bounded-output stable [49], and instability due to time delay is unlikely in these systems [50].

The total Life Cycle Cost (LCC) of the structures includes the initial construction or retrofit cost, the maintenance cost, and the seismic-induced damage costs. When using control systems, although the initial installation and maintenance costs of the control system add up, the total LCC is reduced because the seismic-induced damage costs are diminished by a larger extent. The LCC analysis of controlled structural systems has been performed by researchers to compare various smart systems and quantify the immediate and long-term impacts.

Risk-based probabilistic LCC analysis of controlled structures has proven the cost benefits of control systems [51]. Micheli et al. [52] investigated the cost benefits of three passive control systems implemented on a 39-story building structure located in Boston, MA. The authors used friction and viscous dampers in the proposed systems and concluded that the friction damping provides a more cost-effective solution. Semi-active control systems are economically promising as they provide higher performance, compared with passive systems, with a small increase in costs [53]. Pinkaew and Fujino [54] discussed how semi-active control devices are less costly than active dampers. The practical applications and cost performance of active hydraulic actuators were discussed by Yamamoto [55]. Since 1980s, the extensive and continuous application of semi-active and active structural vibration control systems in more than 70 buildings and bridges in Japan [56, 57] implies the economic effectiveness of this methodology. Cost analysis of smart TMDs installed on a 60-story reinforced concrete building showed that the total cost contribution of the semi-active device to the total construction cost of the building is only 2.0%. In terms of maintenance, the contribution of the control system is less than 0.2% of the total construction cost [58]. Other widespread applications of semi-active systems in bridges [59], including semi-active variable friction dampers on a highway bridge in Oklahoma [60], implies the cost-effective performance of these systems.

5. RESULTS

To evaluate the performance of the proposed load balancing strategy, the calculated input voltage of MR dampers obtained through RDC 1 and considering Chi-Chi earthquake is demonstrated in Figure 9(a). A typical value of V_{max} =10 V is considered as the maximum input voltage capacity for each MR damper [46]. Figure 9(b) shows how the load balance strategy reduces the voltage of overloaded devices and redistributes the additional available voltage over other control devices based on their fitness functions. In order to present Figure 9 with more details and track the changes in voltage more accurately, a close-up version of Figure 9 with the vertical and horizontal axes ranges are limited, is

presented in Figure 14 in Appendix A.

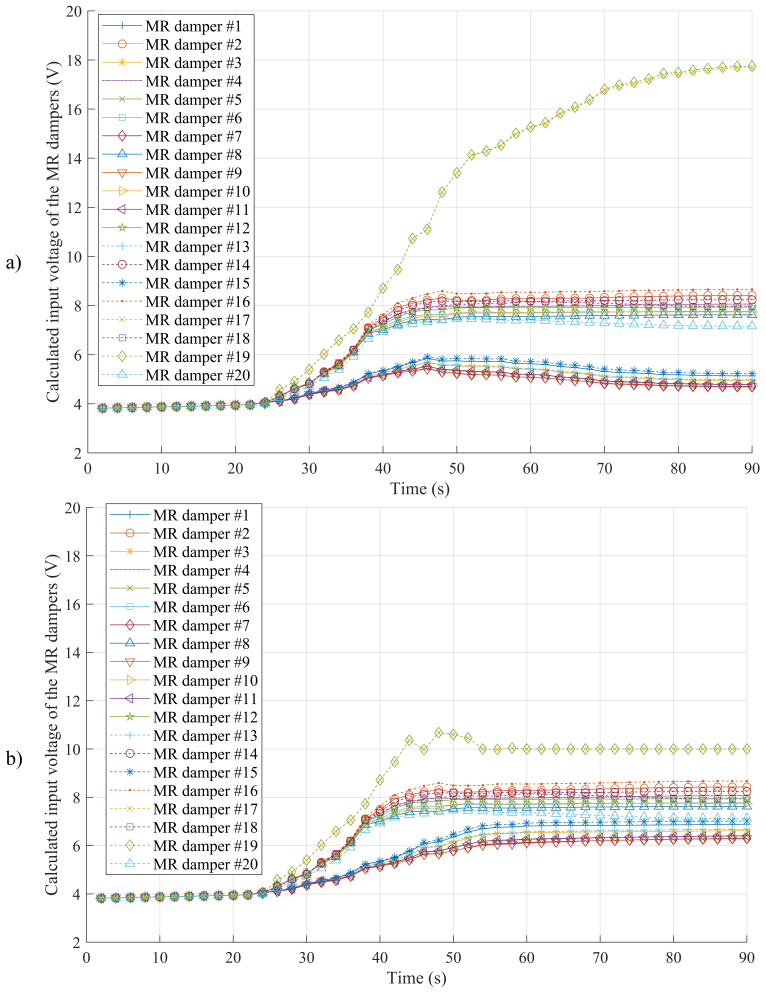

Figure 9: Variation of calculated input voltage of MR dampers obtained from the RDC 1 a) without load balancing b) with load balancing strategy, subjected to Chi-Chi earthquake accelerogram

The relative displacement of the deck at midspan in x direction for three different systems subjected to Chi-Chi earthquake is shown in Figure 10. The systems include: the isolated bridge without MR dampers, the isolated bridge equipped with RDC 1 without load balancing strategy ($\beta = 0.1$ and $V_T = 150$),

and the isolated bridge equipped with RDC1 with load balancing strategy ($\beta = 0.1$ and $V_T = 80$). β and V_T values for these two cases are the optimal values obtained through a grid search. This example shows that the load balancing strategy improves the performance of the controller and reduces the total required voltage resource.

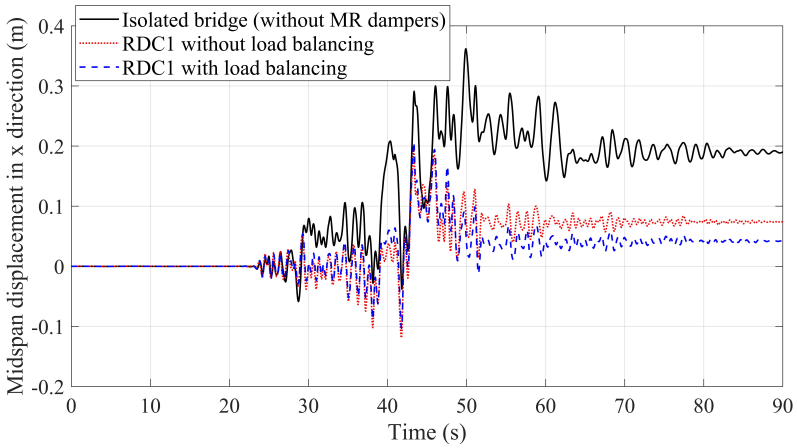

Figure 10: Time history of midspan displacement along x direction in isolated bridge, RDC 1 without load balancing strategy ($\beta = 0.1$ and $V_T = 150$), and RDC1 with load balancing strategy ($\beta = 0.1$ and $V_T = 80$)

In order to optimize V_T and β, the neural dynamic model is implemented and the following results are obtained. Considering a maximum command voltage of 10 V per [46] for each of the 20 MR dampers, the total available voltage is limited to $V_T^{max} = 200$ V. As an example, Figure 11 shows the variation of objective function during the optimization procedure for RDC 3 subjected to Chi-Chi earthquake accelerogram. In general, the objective function follows a descending trend. However, few ascending steps are also observed in Figure 11. The reason is that the ND optimization model uses the gradient of objective function which is calculated separately for each design variable in each iteration. However, when the incremental changes in all design variables are applied together, the variation of objective function may become positive due to the highly nonlinear behavior of the overall system including the bridge and the controller. To avoid

this, one can use smaller λ_m and r_n and repeat more iterations. Herein, as the general descending trend is achieved, λ_m and r_n are not decreased to save computational effort.

Variation of design variables including the growth rate factor and the total available voltage is also demonstrated in Figures 12 and 13. As expected, the design variables gradually converge to the optimal values. The optimal value for V_T is about 50 V which means that on average, the control devices are operating at 25% of their capacity (considering that $V_T = 200$ V when all 20 dampers operate at the maximum capacity, i.e $V_i = 10$ V). According to Figures 11 to 13, the ND model effectively finds the optimal design variables and improves the performance of RDCs. The results of optimization procedure for all controllers and earthquake records are summarized in Table 5. In future research, Monte Carlo simulations with large number of earthquake records will be conducted to further enhance the robustness of the proposed control strategy along with risk assessment and uncertainty analyses [40]. Moreover, the optimal parameters can be used to train deep learning systems to enhance the proposed adaptive data-driven controllers.

Table 5: The optimal design variables for different RDCs subjected to earthquake records

EQ	Design variables	Initial value	Final values obtained through optimization				
			RDC 1	RDC 2	RDC 3	RDC 4	RDC 5
Chi-Chi	V_T	100.0	94.59	34.29	49.98	100.69	98.88
	β	0.1	1.21	0.81	2.50	0.22	0.29
Imperial Valley	V_T	100.0	99.96	95.68	100.08	110.35	91.74
	β	0.1	0.01	0.18	0.11	0.71	0.13
Duzce, Turkey	V_T	100.0	66.31	86.04	74.30	72.70	73.74
	β	0.1	0.72	0.33	2.61	0.50	0.57
Kobe	V_T	100.0	92.01	60.20	100.68	74.39	73.74
	β	0.1	0.25	0.81	0.18	0.64	0.57

The performance criteria resulted from the control systems with optimal variables are compared in Tables 6 to 9. According to the results, the proposed

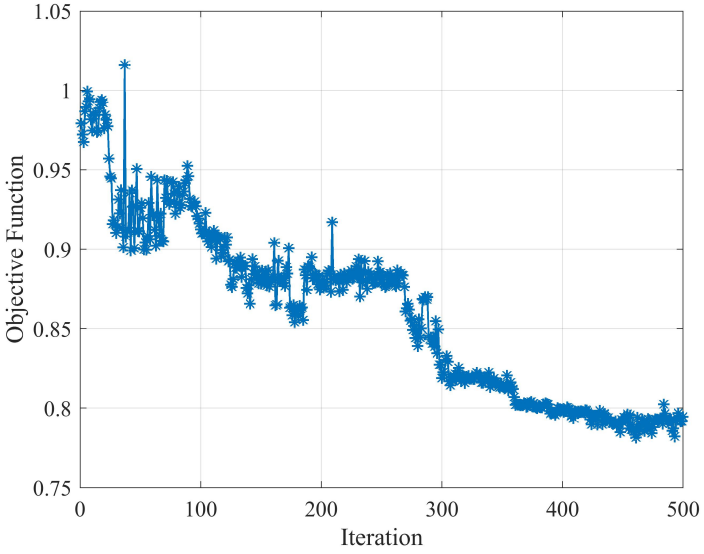

Figure 11: Variation of objective function during the optimization procedure for RDC 3 subjected to Chi-Chi earthquake accelerogram

RDCs show a high performance in reducing the seismic response of the bridge. According to J_1 values in Table 7 and J_9 values in Table 8, using the proposed RDCs, the peak and normed values of the base shear are respectively reduced by up to 41 and 71% with respect to the isolated bridge without MR dampers. The corresponding reductions in the peak and normed overturning moments are 42% and 71%. J_3 and J_{11} values in Tables 7 and 8 also show that RDC1 effectively reduces the peak and normed displacement responses at the midspan by up to 77% and 90%, respectively. J_{15} in Table 9 reveals that RDC3 can reduce the maximum control force in MR dampers by up to 42% compared with Lyapunov controller. Moreover, according to J_{11} and J_{13} in Table 6, RDC3 is capable of reducing the normed midspan displacement and bearing deformation by up to 52 % compared to the Lyapunov controller.

In general, RDCs show a higher performance in reducing the peak and normed values of base shear, overturning moment, mid-span displacement, bearing deformation, and column curvature, compared to the mid-span acceleration.

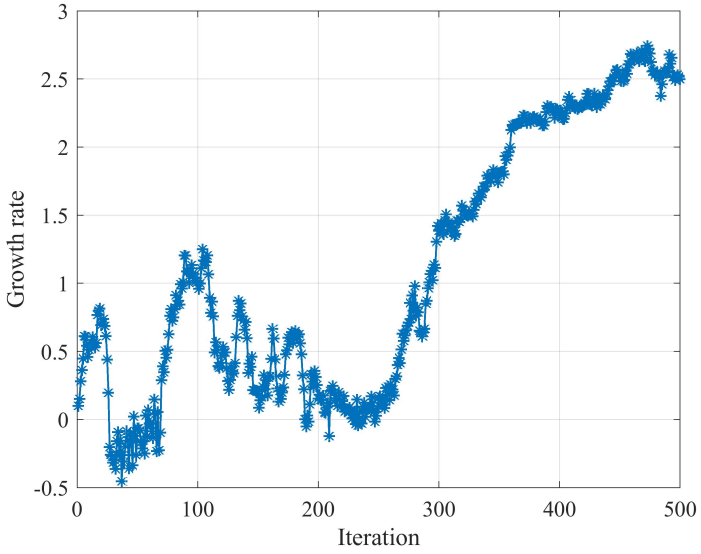

Figure 12: Variation of the growth rate during the optimization procedure for RDC 3 subjected to Chi-Chi earthquake accelerogram

Considering the output data presented for J_4 and J_{12}, all the control systems increase the peak and normed values of mid-span acceleration. The reason is that the MR dampers increase the overall rigidity of the connection between the deck and the bent columns. Consequently, more inertial force is transferred to the deck and the deck vibrates with a higher acceleration. The fuzzy controller is effective in avoiding highly increased accelerations since the rule-base is sensitive to the variation of velocity. Among the proposed RDCs, RDC1, RDC2, and RDC3 show a more satisfactory performance to reduce the acceleration response and inertial force in the deck. One of the most important factors affecting the maintenance costs related to isolation bearings is the peak and normed values of deformation in bearings. Considering the results obtained for J_5 and J_{13}, the proposed controllers more effectively reduce the bearing deformation in isolators, compared with the Lyapunov and fuzzy controllers.

The Lyapunov controller is model-based and relies on structural properties of the bridge. This leads to a reduced robustness due to the uncertainties in the

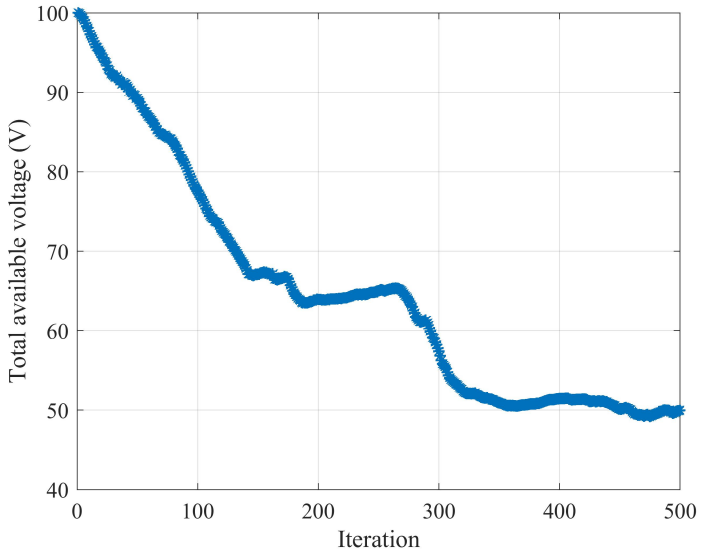

Figure 13: Variation of the total available voltage during the optimization procedure for RDC 3 subjected to Chi-Chi earthquake accelerogram

stiffness and mass matrices as well as the variation of these matrices due to the geometrical and material nonlinearities in real world. On the other hand, the proposed RDCs only rely on the measured data and show robust performance against system uncertainties. Investigation on the LCCs specific to the proposed system is an open subject for future research which requires detailed procurement, installation, and maintenance cost information related to the control system components. Future directions of this research also include validating the proposed RDCs using novel testing technology of real-time hybrid simulation of bridge structures equipped with semi-active dampers [61].

6. CONCLUSION

A new design of Replicator Dynamic Controllers (RDCs) integrated with a load balancing strategy for semi-active vibration control of bridge structures was investigated in the present study. Five RDCs with different fitness functions were proposed for controlling the performance of 20 MR dampers installed on an isolated highway bridge. The bridge was simulated based on the benchmark

Table 6: Performance criteria of different control systems subjected to Chi-Chi earthquake (best result is shown in **bold**)

Criteria	RDC 1	RDC 2	RDC 3	RDC 4	RDC 5	Fuzzy	Lyapunov
J_1	1.0511	0.7867	**0.7458**	1.0649	1.0568	0.7981	0.9154
J_2	1.0436	0.9199	**0.7905**	1.0652	1.0333	0.8850	0.8869
J_3	0.9220	0.9183	0.8457	0.8743	0.8812	0.8058	**0.7410**
J_4	1.4855	**1.0861**	1.1697	1.4559	1.4256	1.2776	1.1338
J_5	0.9117	0.9150	0.8396	0.8646	0.8712	0.7999	**0.7444**
J_6	1.0436	0.9199	**0.7905**	1.0652	1.0333	0.8850	0.8869
J_7	0.0000	0.0000	0.0000	0.0000	0.0000	0.0000	0.0000
J_8	0.0000	0.0000	0.0000	0.0000	0.0000	0.0000	0.0000
J_9	0.8914	1.0023	**0.6795**	0.8626	0.8584	0.6918	1.0050
J_{10}	0.8817	0.9862	**0.6709**	0.8517	0.8484	0.6908	0.9964
J_{11}	0.6225	1.0682	**0.4392**	0.5909	0.5854	0.6189	0.9044
J_{12}	2.0169	**1.3955**	1.5616	2.0736	2.0631	1.4054	1.5845
J_{13}	0.6270	1.1040	**0.4327**	0.5951	0.5850	0.6182	0.9060
J_{14}	0.8817	0.9862	0.6709	0.8517	0.8484	**0.6908**	0.9964
J_{15}	0.0052	0.0049	0.0050	0.0052	0.0051	**0.0048**	0.0051
J_{16}	0.9117	0.9150	**0.8396**	0.8646	0.8712	0.7999	0.7444
J_{17}	NaN	NaN	NaN	NaN	NaN	NaN	NaN
J_{18}	NaN	NaN	NaN	NaN	NaN	NaN	NaN
J_{19}	20	20	20	20	20	20	20
J_{20}	40	40	40	40	40	40	40
J_{21}	28	28	28	28	28	28	28

control problem of 91/5 highway bridge in Southern California subjected to near-field earthquake records. The RDCs were configured to allocate the total available voltage to the current drivers of the MR dampers. The allocation of total voltage/current was then modified using a load balancing strategy intended to reallocate additional voltage considering a maximum voltage to the current

Table 7: Performance criteria of different control systems subjected to Imperial Valley earthquake (best result is shown in **bold**)

Criteria	RDC 1	RDC 2	RDC 3	RDC 4	RDC 5	Fuzzy	Lyapunov
J_1	0.6211	**0.5884**	0.6241	0.7095	0.6040	0.5800	0.7608
J_2	0.5843	0.5761	0.5817	0.7226	0.5992	**0.5612**	0.7107
J_3	0.3331	0.3244	0.3377	**0.2742**	0.3141	0.5361	0.3647
J_4	1.6201	1.6387	1.6196	1.7727	1.6654	**1.2957**	1.3530
J_5	0.3375	0.3241	0.3407	**0.2552**	0.3042	0.5674	0.3458
J_6	0.5843	0.5761	0.5817	0.7226	0.5992	**0.5612**	0.7107
J_7	0.0000	0.0000	0.0000	0.0000	0.0000	0.0000	0.0000
J_8	0.0000	0.0000	0.0000	0.0000	0.0000	0.0000	0.0000
J_9	0.6597	0.6499	0.6590	0.7696	0.6832	0.7834	**0.5352**
J_{10}	0.6527	0.6416	0.6522	0.7599	0.6749	0.7785	**0.5122**
J_{11}	0.4382	0.4122	0.4394	**0.1265**	0.3821	0.7265	0.3244
J_{12}	1.3466	1.3971	1.3427	1.5353	1.4021	**1.0638**	1.2323
J_{13}	0.4607	0.4246	0.4604	**0.1243**	0.3846	0.7643	0.3314
J_{14}	0.6527	0.6416	0.6522	0.7599	0.6749	0.7785	**0.5122**
J_{15}	0.0030	0.0048	0.0027	0.0050	0.0044	**0.0018**	0.0050
J_{16}	0.3375	0.3241	0.3407	**0.2552**	0.3042	0.5674	0.3458
J_{17}	NaN	NaN	NaN	NaN	NaN	NaN	NaN
J_{18}	NaN	NaN	NaN	NaN	NaN	NaN	NaN
J_{19}	20	20	20	20	20	20	20
J_{20}	40	40	40	40	40	40	40
J_{21}	28	28	28	28	28	28	28

driver for each MR damper. The patented Neural Dynamic (ND) model of Adeli and Park incorporating the Lyapunov stability theorem and the Karush-Kuhn-Tucker conditions were utilized to optimize the control parameters, including the total available voltage and the growth rate of the replicator. The performance of the proposed controllers was compared with conventional Lyapunov

Table 8: Performance criteria of different control systems subjected to Duzce earthquake (best result is shown in **bold**)

Criteria	RDC 1	RDC 2	RDC 3	RDC 4	RDC 5	Fuzzy	Lyapunov
J_1	0.7837	0.7921	0.8031	1.1583	1.1582	**0.6617**	0.8265
J_2	0.8333	0.8213	0.8324	1.1954	1.1954	**0.7175**	0.8684
J_3	0.5465	0.5554	0.5506	0.4955	0.4931	0.5647	**0.3639**
J_4	1.0060	1.1555	1.0464	1.2307	1.2397	**1.0045**	1.1494
J_5	0.5161	0.5307	0.5233	0.5112	0.5086	0.5348	**0.3814**
J_6	0.8333	0.8213	0.8324	1.1954	1.1954	**0.7175**	0.8684
J_7	0.0000	0.0000	0.0000	0.0000	0.0000	0.0000	0.0000
J_8	0.0000	0.0000	0.0000	0.0000	0.0000	0.0000	0.0000
J_9	0.3017	**0.2885**	0.2999	0.4199	0.4282	0.4818	0.4290
J_{10}	0.2980	**0.2853**	0.2963	0.4173	0.4260	0.4795	0.4216
J_{11}	**0.0989**	0.1354	0.1012	0.2959	0.3116	0.3967	0.3191
J_{12}	1.1399	1.2557	1.1569	1.2344	1.2477	**0.9369**	1.1278
J_{13}	**0.0943**	0.1315	0.0958	0.2949	0.3109	0.3966	0.3360
J_{14}	0.2980	**0.2853**	0.2963	0.4173	0.4260	0.4795	0.4216
J_{15}	0.0050	0.0049	0.0049	**0.0037**	0.0040	0.0039	0.0050
J_{16}	0.5161	0.5307	0.5233	0.5112	0.5086	0.5348	**0.3814**
J_{17}	NaN	NaN	NaN	NaN	NaN	NaN	NaN
J_{18}	NaN	NaN	NaN	NaN	NaN	NaN	NaN
J_{19}	20	20	20	20	20	20	20
J_{20}	40	40	40	40	40	40	40
J_{21}	28	28	28	28	28	28	28

and fuzzy control algorithms in terms of 21 different performance criteria describing the reductions in dynamic response of the bridge. The proposed fuzzy controller uses a rule-base focusing on the relative velocity across the damper to determine the command voltage. The results showed that the ND optimization procedure effectively optimizes the controller performance and achieves the

Table 9: Performance criteria of different control systems subjected to Kobe earthquake (best result is shown in **bold**)

Criteria	RDC 1	RDC 2	RDC 3	RDC 4	RDC 5	Fuzzy	Lyapunov
J_1	0.7884	**0.6939**	0.7407	0.7754	0.7203	0.8899	0.8922
J_2	0.8974	**0.7453**	0.8437	0.8322	0.8014	0.8817	0.8548
J_3	**0.2350**	0.2695	0.3154	0.3108	0.2788	0.6852	0.2609
J_4	2.2204	2.2090	2.0606	2.2950	2.1843	**1.4457**	1.9050
J_5	**0.2259**	0.2619	0.3051	0.3010	0.2715	0.6752	0.2659
J_6	0.8974	**0.7453**	0.8437	0.8322	0.8014	0.8817	0.8548
J_7	0.0000	0.0000	0.0000	0.0000	0.0000	0.0000	0.0000
J_8	0.0000	0.0000	0.0000	0.0000	0.0000	0.0000	0.0000
J_9	0.5785	**0.4681**	0.5209	0.5294	0.5079	0.8989	0.5257
J_{10}	0.5726	**0.4623**	0.5150	0.5238	0.5019	0.8909	0.5165
J_{11}	**0.1352**	0.2221	0.1558	0.2067	0.1568	0.8146	0.2777
J_{12}	1.4753	1.5379	1.3768	1.5093	1.4950	**1.0847**	1.1916
J_{13}	**0.1174**	0.2074	0.1373	0.2079	0.1577	0.8168	0.2799
J_{14}	0.5726	**0.4623**	0.5150	0.5238	0.5019	0.8909	0.5165
J_{15}	0.0050	0.0049	**0.0029**	0.0039	0.0039	**0.0029**	0.0050
J_{16}	**0.2259**	0.2619	0.3051	0.3010	0.2715	0.6752	0.2659
J_{17}	NaN	NaN	NaN	NaN	NaN	NaN	NaN
J_{18}	NaN	NaN	NaN	NaN	NaN	NaN	NaN
J_{19}	20	20	20	20	20	20	20
J_{20}	40	40	40	40	40	40	40
J_{21}	28	28	28	28	28	28	28

optimal design variables. The optimal RDCs also showed a significant performance in improving the dynamic response of the bridge including the peak and normed values of base shear, overturning moment, mid-span displacement, bearing deformation, column curvature, dissipated energy, and the number of plastic hinges. The proposed fuzzy controller showed acceptable performance to avoid

major increases in acceleration response.

7. ACKNOWLEDGEMENT

The authors would like to acknowledge Professor Hojjat Adeli and Professor Hyo Seon Park's permission to use the patented Neural Dynamic model during the optimization section of this paper.

8. APPENDIX A

Table 10: Description of different performance criteria used to evaluate the effectiveness of controllers (adapted from Agrawal et al. [45])

Criterion	Description	Formula
J_1	Peak base shear in controlled state normalized by the corresponding value in uncontrolled state	$\frac{\max \lvert F_b(t) \rvert}{F_{0b}^{max}}$
J_2	Peak overturning moment in controlled state normalized by the corresponding value in uncontrolled state	$\frac{\max \lvert M_b(t) \rvert}{M_{0b}^{max}}$
J_3	Peak mid-span displacement in controlled state normalized by the corresponding value in uncontrolled state	$\frac{\max \lvert u_{deck}(t) \rvert}{u_{0deck}^{max}}$
J_4	Peak mid-span acceleration in controlled state normalized by the corresponding value in uncontrolled state	$\frac{\max \lvert \ddot{u}_{deck}(t) \rvert}{\ddot{u}_{0deck}^{max}}$
J_5	Peak bearing deformation in controlled state normalized by the corresponding value in uncontrolled state	$\frac{\max \lvert y_b(t) \rvert}{y_{0b}^{max}}$
J_6	Peak bent column curvature in controlled state normalized by the corresponding value in uncontrolled state	$\frac{\max \lvert \phi_b(t) \rvert}{\phi_{0b}^{max}}$
J_7	Peak dissipated energy at bent column in controlled state normalized by the corresponding value in uncontrolled state	$\frac{\max E_b}{E_{0b}^{max}}$
J_8	Number of plastic hinges in controlled state normalized by the corresponding value in uncontrolled state	$\frac{N_d^c}{N_d}$

J_9	Normed base shear in controlled state normalized by the corresponding value in uncontrolled state	$\frac{\|F_b(t)\|}{\|F_{0b}^{max}\|}$
J_{10}	Normed overturning moment in controlled state normalized by the corresponding value in uncontrolled state	$\frac{\|M_b(t)\|}{\|M_{0b}^{max}\|}$
J_{11}	Normed mid-span displacement in controlled state normalized by the corresponding value in uncontrolled state	$\frac{\|u_{deck}(t)\|}{\|u_{0deck}^{max}\|}$
J_{12}	Normed mid-span acceleration in controlled state normalized by the corresponding value in uncontrolled state	$\frac{\|\ddot{u}_{deck}(t)\|}{\|\ddot{u}_{0deck}^{max}\|}$
J_{13}	Normed bearing deformation in controlled state normalized by the corresponding value in uncontrolled state	$\frac{\|y_b(t)\|}{\|y_{0b}^{max}\|}$
J_{14}	Normed bent column curvature in controlled state normalized by the corresponding value in uncontrolled state	$\frac{\|\phi_b(t)\|}{\|\Phi_{0b}^{max}\|}$
J_{15}	Peak control force in MR dampers normalized by the mass of superstructure	$\frac{\max\|F_c(t)\|}{W_b}$
J_{16}	Peak stroke of the MR dampers normalized by the maximum peak bearing deformation in the uncontrolled structures	$\frac{\max d_s}{y_{0b}^{max}}$
J_{17}	Peak instantaneous power required by the MR dampers normalized by the product of the weight and the peak bearing velocity in the uncontrolled state	$\frac{\max\sum P_c(t)\|}{\dot{y}_{0b}^{max}W_b}$
J_{18}	Peak total power required for all MR dampers normalized by the product of the weight and the peak bearing deformation in the uncontrolled state	$\frac{\max\int P_c(t)\|}{\dot{y}_{0b}^{max}W_b})$
J_{19}	Number of MR dampers	-
J_{20}	Number of sensors	-
J_{21}	Dimension of the discrete state vector required for the control algorithm	-

490

a)

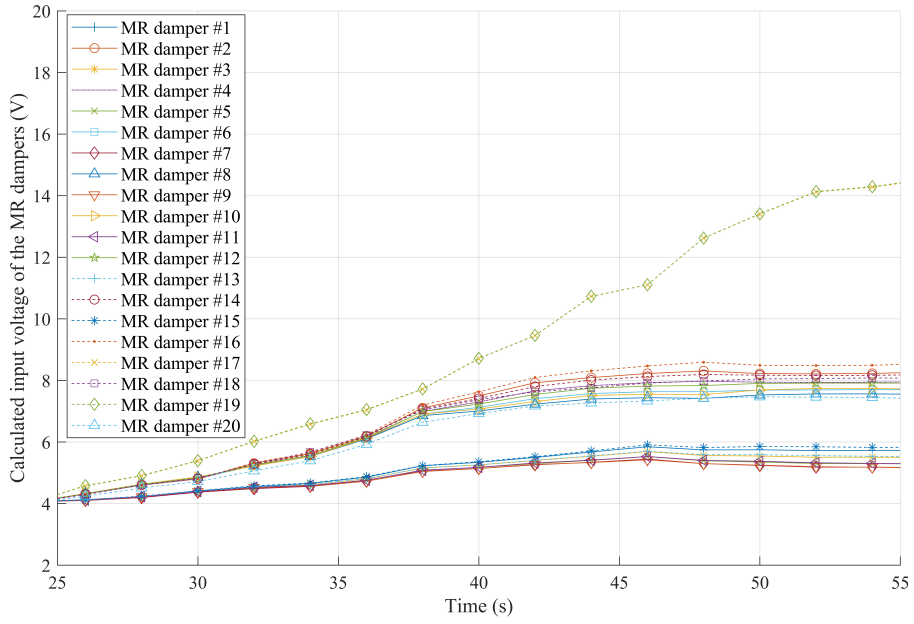

b)

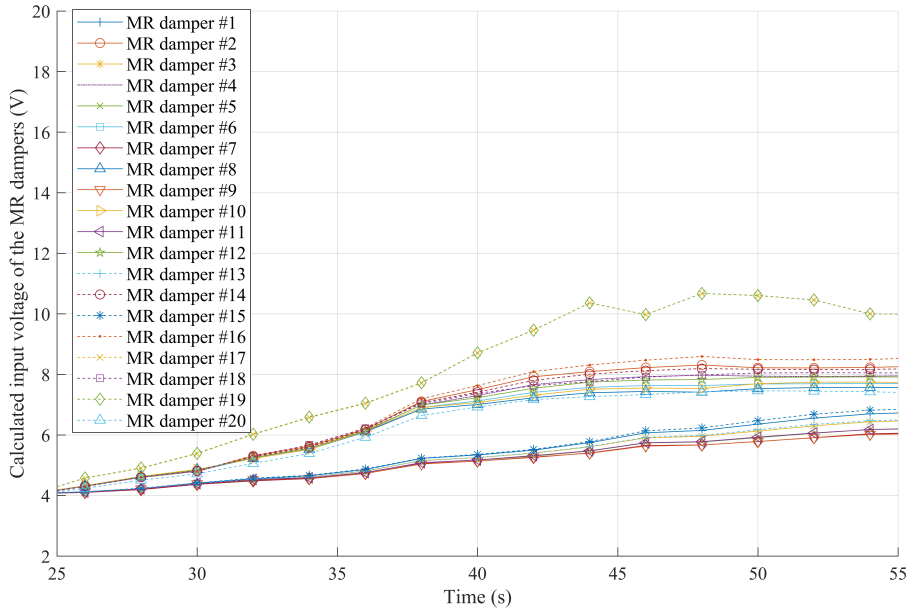

Figure 14: Detailed variation of calculated input voltage of MR dampers obtained from RDC1 a) without load balancing b) with load balancing strategy, subjected to Chi-Chi earthquake

9. APPENDIX B

The following is the list of notations together with the related values and units considered in the present study.

$\mathbf{A}$ = system matrix in state space model;
A_m = constant value affecting the evolutionary variable (1.2);
$\mathbf{B}_r$ = control force matrices corresponding to $\mathbf{z}_r(t)$;
$\mathbf{B}_w$ = control force matrices corresponding to $\mathbf{z}_w(t)$;
$\mathbf{C}$ = bridge damping matrix;
C_0 = velocity coefficient affecting the damping force (N.s/cm));
C_{0a} = first coefficient affecting C_0 (4.40 N.s/cm);
C_{0b} = second coefficient affecting C_0 (44.0 N.s/(cm.V));
$\mathbf{D}$ = feedforward matrix affecting the control forces vector;
$\mathbf{E}$ = input force vector corresponding to the ground acceleration;
F = objective function;
F_d = damping force of MR damper (N);
G = total number of inequality constraints;
G_b = modulation constant for the load balancing strategy;
$\mathbf{K}$ = bridge stiffness matrix;
K = total number of equality constraints;
$\mathbf{L}_g$ = feedforward vector affecting the ground acceleration term;
L = Lagrange function;
$\mathbf{M}$ = bridge mass matrix;
M = size of design variable vector;
N = total number of MR dampers;
N_c = number of proposed RDCs (5);
$Q_i^{(j)}$ = measurement at the i^{th} location using the j^{th} controller;
$\mathbf{R}$ = influence matrix affecting the semi-active control force, $\mathbf{r}$(t);
$\mathbf{T}$ = output matrix in state space model;
V_e = additional available voltage (V);
V_i = command voltage to the current driver of the i^{th} MR damper (V);
V_i^m = modified command voltage to the i^{th} MR damper (V);
V_{max} = maximum input voltage capacity of MR dampers (V);

V_T = total available voltage (V);

$\mathbf{W}$ = influence matrix affecting the passive (isolation) control force, $\mathbf{w}$(t);

a = coefficient acting on the evolutionary variable (N/cm);

a_a = first coefficient affecting a (1.0872×10^5 N/cm);

a_b = second coefficient affecting a (4.9616×10^5 N/(cm.V));

f_i = fitness function for the i^{th} MR damper;

$f_i^{(j)m}$ = modified fitness function for the i^{th} MR damper in the j^{th} controller;

h_k = k^{th} equality constraint;

j = number of inequality constraint;

k = number of equality constraint;

n = order of the evolutionary variable equation (1.0);

n_i = iteration number in the optimization algorithm;

$\mathbf{r}$ = semi-active control force vector;

r_0 = initial penalty parameter;

r_n = exterior penalty parameter;

$\mathbf{u}$ = bridge displacement vector;

$\ddot{u}_g$ = ground acceleration;

g_j = j^{th} inequality constraint;

t = time (s);

u = displacement response (m);

$\mathbf{v}$ = population vector in replicator dynamic model;

$\mathbf{w}$ = passive (isolation) control force vector;

$\mathbf{x}$ = state space variable vector;

$\mathbf{y}$ = output vector in state space model;

$\mathbf{z}$ = design variable vector;

z_d = evolutionary variable;

$\mathbf{z}_r$ = semi-active control force vector in state space model;

$\mathbf{z}_w$ = passive control force vector in state space model;

$\boldsymbol{\theta}$ = inertial force distribution vector;

α = Lagrange multiplier for inequality constraint term;

β = growth rate in replicator dynamic model;

β_d = constant value affecting the evolutionary variable (3.0 cm^{-1});

γ = Lagrange multiplier for equality constraint term;

γ_d = constant value affecting the evolutionary variable (3.0 cm^{-1});

ϵ = strictly positive number used to obtain penalty parameter;

η = time lag constant (50.0 s^{-1});

λ = Lagrange multiplier for objective function term;

ν = applied control voltage to the current driver (V);

ϕ = weighted average of fitness functions;

ϕ^m = modified averaged fitness function;

ω_j = square root of absolute value of $g_j(\mathbf{x})$;

∇ = the gradient of a function;

References

[1] N. L. Dehghani, Y. M. Darestani, A. Shafieezadeh, Optimal life-cycle resilience enhancement of aging power distribution systems: A minlp-based preventive maintenance planning, IEEE Access 8 (2020) 22324–22334.

[2] S. Zamanian, B. Terranova, A. Shafieezadeh, Significant variables affecting the performance of concrete panels impacted by wind-borne projectiles: A global sensitivity analysis, International Journal of Impact Engineering (2020) 103650.

[3] K. Wardhana, F. C. Hadipriono, Analysis of recent bridge failures in the united states, Journal of performance of constructed facilities 17 (3) (2003) 144–150.

[4] Y. T. Hsu, C. C. Fu, Seismic effect on highway bridges in chi chi earthquake, Journal of performance of constructed facilities 18 (1) (2004) 47–53.

[5] Q. Han, X. Du, J. Liu, Z. Li, L. Li, J. Zhao, Seismic damage of highway bridges during the 2008 wenchuan earthquake, Earthquake Engineering and Engineering Vibration 8 (2) (2009) 263–273.

[6] M. Kunde, R. Jangid, Seismic behavior of isolated bridges: A-state-of-the-art review, Electronic Journal of Structural Engineering 3 (2) (2003) 140–169.

[7] N. Makris, Seismic isolation: Early history, Earthquake Engineering & Structural Dynamics 48 (2) (2019) 269–283.

[8] M. H. Stanikzai, S. Elias, V. A. Matsagar, A. K. Jain, Seismic response control of base-isolated buildings using tuned mass damper, Australian Journal of Structural Engineering 21 (1) (2020) 310–321.

[9] I. G. Buckle, M. C. Constantinou, M. Diceli, H. Ghasemi, Seismic isolation of highway bridges, Tech. Rep. No. MCEER-06-SP07 (2006).

[10] K. Ghaedi, Z. Ibrahim, H. Adeli, A. Javanmardi, Invited review: Recent developments in vibration control of building and bridge structures, Journal of Vibroengineering 19 (5) (2017) 3564–3580.

[11] M. Gutierrez Soto, H. Adeli, Semi-active vibration control of smart isolated highway bridge structures using replicator dynamics, Engineering Structures 186 (2019) 536–552.

[12] C. W. De Silva, Intelligent control: fuzzy logic applications, CRC press, 1995.

[13] M. D. Symans, S. W. Kelly, Fuzzy logic control of bridge structures using intelligent semi-active seismic isolation systems, Earthquake Engineering & Structural Dynamics 28 (1) (1999) 37–60.

[14] K.-S. Park, H.-M. Koh, S.-Y. Ok, C.-W. Seo, Fuzzy supervisory control of earthquake-excited cable-stayed bridges, Engineering Structures 27 (7) (2005) 1086–1100.

[15] S.-Y. Ok, D.-S. Kim, K.-S. Park, H.-M. Koh, Semi-active fuzzy control of cable-stayed bridges using magneto-rheological dampers, Engineering structures 29 (5) (2007) 776–788.

[16] S. Salari, S. J. Hormozabad, A. K. Ghorbani-Tanha, M. Rahimian, Innovative mobile tmd system for semi-active vibration control of inclined sagged cables, KSCE Journal of Civil Engineering 23 (2) (2019) 641–653.

[17] N. Wang, H. Adeli, Self-constructing wavelet neural network algorithm for nonlinear control of large structures, Engineering Applications of Artificial Intelligence 41 (2015) 249–258.

[18] J. Zhang, A. K. Agrawal, An innovative hardware emulated simple passive semi-active controller for vibration control of mr dampers, Smart Structures and Systems 15 (3) (2015) 831–846.

[19] M. AlHamaydeh, M. A. Jaradat, M. Serry, L. Sawaqed, K. S. Hatamleh, Structural control of mr-dampers with genetic algorithm-optimized quasi-bang-bang controller, in: 2017 7th International Conference on Modeling, Simulation, and Applied Optimization (ICMSAO), IEEE, 2017, pp. 1–6.

[20] S. J. Hormozabad, A. K. Ghorbani-Tanha, Semi-active fuzzy control of lali cable-stayed bridge using mr dampers under seismic excitation, Frontiers of Structural and Civil Engineering 14 (3) (2020) 706–721.

[21] R. W Soares, L. R. Barroso, O. AS Al-Fahdawi, Adaptive control for response attenuation of seismically excited cable-stayed bridges, Journal of Vibration and Control 26 (3-4) (2020) 131–145.

[22] A. Yanik, U. Aldemir, A simple structural control model for earthquake excited structures, Engineering Structures 182 (2019) 79–88.

[23] Y. Xie, C. Wang, H. Shi, J. Shi, A data driven control method for structure vibration suppression, Acta Astronautica 143 (2018) 302–309.

[24] Z.-S. Hou, Z. Wang, From model-based control to data-driven control: Survey, classification and perspective, Information Sciences 235 (2013) 3–35.

[25] W. Song, S. Dyke, Real-time dynamic model updating of a hysteretic structural system, Journal of Structural Engineering 140 (3) (2014) 04013082.

[26] Y. Zhang, M. Guizani, Game theory for wireless communications and networking, CRC press, 2011.

[27] D. Bauso, Game theory with engineering applications, SIAM, 2016.

[28] J. R. Marden, J. S. Shamma, Game theory and distributed control, in: Handbook of game theory with economic applications, Vol. 4, Elsevier, 2015, pp. 861–899.

[29] M. Elhenawy, A. A. Elbery, A. A. Hassan, H. A. Rakha, An intersection game-theory-based traffic control algorithm in a connected vehicle environment, in: 2015 IEEE 18th international conference on intelligent transportation systems, IEEE, 2015, pp. 343–347.

[30] I. A. Villalobos, A. S. Poznyak, A. M. Tamayo, Urban traffic control problem: a game theory approach, IFAC Proceedings Volumes 41 (2) (2008) 7154–7159.

[31] M. Gutierrez Soto, Bio-inspired hybrid vibration control methodology for intelligent isolated bridge structures, in: Active and Passive Smart Structures and Integrated Systems XII, Vol. 10595, International Society for Optics and Photonics, 2018, p. 1059511.

[32] M. Gutierrez Soto, H. Adeli, Vibration control of smart base-isolated irregular buildings using neural dynamic optimization model and replicator dynamics, Engineering Structures 156 (2018) 322–336.

[33] H. Adeli, H. S. Park, Optimization of space structures by neural dynamics, Neural networks 8 (5) (1995) 769–781.

[34] H. Adeli, H. S. Park, Neurocomputing for design automation, CRC Press, 1998.

[35] M. Gutierrez Soto, H. Adeli, Many-objective control optimization of high-rise building structures using replicator dynamics and neural dynamics model, Structural and Multidisciplinary Optimization 56 (6) (2017) 1521–1537.

[36] M. K. Sohrabi, H. Azgomi, A survey on the combined use of optimization methods and game theory, Archives of Computational Methods in Engineering 27 (1) (2020) 59–80.

[37] S. Banerjee, J. P. Hecker, A multi-agent system approach to load-balancing and resource allocation for distributed computing, in: First Complex Systems Digital Campus World E-Conference 2015, Springer, 2017, pp. 41–54.

[38] A. A. Neghabi, N. J. Navimipour, M. Hosseinzadeh, A. Rezaee, Load balancing mechanisms in the software defined networks: a systematic and comprehensive review of the literature, IEEE Access 6 (2018) 14159–14178.

[39] J. E. Brommer, The evolution of fitness in life-history theory, Biological Reviews 75 (3) (2000) 377–404.

[40] M. Gutierrez Soto, H. Adeli, Multi-agent replicator controller for sustainable vibration control of smart structures, Journal of Vibroengineering 19 (2017) 4300–4322.

[41] J. Xia, J. Zhang, J. Feng, Z. Wang, G. Zhuang, Command filter-based adaptive fuzzy control for nonlinear systems with unknown control directions, IEEE Transactions on Systems, Man, and Cybernetics: Systems (2019).

[42] M. Aldwaik, H. Adeli, Advances in optimization of highrise building structures, Structural and Multidisciplinary Optimization 50 (6) (2014) 899–919.

[43] M. Aldwaik, H. Adeli, Cost optimization of reinforced concrete flat slabs of arbitrary configuration in irregular highrise building structures, Structural and Multidisciplinary Optimization 54 (1) (2016) 151–164.

[44] S. Nagarajaiah, S. Narasimhan, A. Agrawal, P. Tan, Benchmark structural control problem for a seismically excited highway bridge—part iii: Phase ii sample controller for the fully base-isolated case, Structural Control and Health Monitoring: The Official Journal of the International Association for Structural Control and Monitoring and of the European Association for the Control of Structures 16 (5) (2009) 549–563.

[45] A. Agrawal, P. Tan, S. Nagarajaiah, J. Zhang, Benchmark structural control problem for a seismically excited highway bridge—part i: Phase i problem definition, Structural Control and Health Monitoring: The Official Journal of the International Association for Structural Control and Monitoring and of the European Association for the Control of Structures 16 (5) (2009) 509–529.

[46] L. M. Jansen, S. J. Dyke, Semiactive control strategies for mr dampers: comparative study, Journal of engineering mechanics 126 (8) (2000) 795–803.

[47] F. Yi, S. J. Dyke, J. M. Caicedo, J. D. Carlson, Experimental verification of multiinput seismic control strategies for smart dampers, Journal of Engineering Mechanics 127 (11) (2001) 1152–1164.

[48] P. Tan, A. K. Agrawal, Benchmark structural control problem for a seismically excited highway bridge—part ii: phase i sample control designs, Structural Control and Health Monitoring: The Official Journal of the International Association for Structural Control and Monitoring and of the European Association for the Control of Structures 16 (5) (2009) 530–548.

[49] S. Dyke, B. Spencer Jr, M. Sain, J. Carlson, Modeling and control of magnetorheological dampers for seismic response reduction, Smart materials and structures 5 (5) (1996) 565.

[50] Y. Cha, A. Agrawal, S. Dyke, Time delay effects on large-scale mr damper based semi-active control strategies, Smart Materials and Structures 22 (1) (2012) 015011.

[51] O. El-Khoury, A. Shafieezadeh, E. Fereshtehnejad, A risk-based life cycle cost strategy for optimal design and evaluation of control methods for nonlinear structures, Earthquake Engineering & Structural Dynamics 47 (11) (2018) 2297–2314.

[52] L. Micheli, A. Alipour, S. Laflamme, P. Sarkar, Performance-based design with life-cycle cost assessment for damping systems integrated in wind excited tall buildings, Engineering Structures 195 (2019) 438–451.

[53] F. Y. Cheng, H. Jiang, K. Lou, Smart structures: innovative systems for seismic response control, CRC press, 2008.

[54] T. Pinkaew, Y. Fujino, Effectiveness of semi-active tuned mass dampers under harmonic excitation, Engineering Structures 23 (7) (2001) 850–856.

[55] M. Yamamoto, S. Aizawa, M. Higashino, K. Toyama, Practical applications of active mass dampers with hydraulic actuator, Earthquake engineering & structural dynamics 30 (11) (2001) 1697–1717.

[56] Y. Ikeda, Active and semi-active vibration control of buildings in japan—practical applications and verification, Structural Control and Health Monitoring: The Official Journal of the International Association for Structural Control and Monitoring and of the European Association for the Control of Structures 16 (7-8) (2009) 703–723.

[57] Y. Fujino, D. M. Siringoringo, Y. Ikeda, T. Nagayama, T. Mizutani, Research and implementations of structural monitoring for bridges and buildings in japan, Engineering 5 (6) (2019) 1093–1119.

[58] K.-T. Tse, K. C. Kwok, Y. Tamura, Performance and cost evaluation of a smart tuned mass damper for suppressing wind-induced lateral-torsional motion of tall structures, Journal of Structural Engineering 138 (4) (2012) 514–525.

[59] K. I. Gkatzogias, A. J. Kappos, Semi-active control systems in bridge engineering: a review of the current state of practice, Structural Engineering International 26 (4) (2016) 290–300.

[60] W. Neff Patten, J. Sun, G. Li, J. Kuehn, G. Song, Field test of an intelligent stiffener for bridges at the i-35 walnut creek bridge, Earthquake engineering & structural dynamics 28 (2) (1999) 109–126.

[61] A. Palacio-Betancur, M. Gutierrez Soto, Adaptive tracking control for real-time hybrid simulation of structures subjected to seismic loading, Mechanical Systems and Signal Processing 134 (2019) 106345.